JPE 17-1-7

https://doi.org/10.6113/JPE.2017.17.1.67
ISSN(Print): 1598-2092 / ISSN(Online): 2093-4718

A New Method for Elimination of Zero-Sequence Voltage in Dual Three-Level Inverter Fed Open-End Winding Induction Motors

Yi-Wen Geng*, Chen-Xi Wei*, Rui-Cheng Chen*, Liang Wang†, Jia-Bin Xu*, and Shuang-Cheng Hao*

*,†School of Information and Electrical Engineering, China University of Mining and Technology, Xuzhou, China

Abstract

Due to the excessive zero-sequence voltage in dual three-level inverter fed open-end winding induction motor systems, zero-sequence circumfluence which is harmful to switching devices and insulation is then formed when operating in a single DC voltage source supplying mode. Traditionally, it is the mean value instead of instantaneous value of the zero-sequence voltage that is eliminated, through adjusting the durations of the operating vectors. A new strategy is proposed for zero-sequence voltage elimination, which utilizes unified voltage modulation and a decoupled SVPWM strategy to achieve two same-sized equivalent vectors for an angle of 120°, generated by two inverters independently. Both simulation and experimental results have verified its efficiency in the instantaneous value elimination of zero-sequence voltage.

Key words: Dual three-level inverter-fed open-end winding induction motor, Space-vector decoupling PWM, Unified pulse width modulation, Zero-sequence voltage

I. INTRODUCTION

Multilevel inverters have been popular in recent years due to their advantages such as reduced output harmonics and reduced voltage derivatives (dv/dt) [1], [2], which are commonly applied in medium and high voltage situations. In the case of an equal number of switching devices, compared with NPC (Neutral Point Clamped) [3], [4], Flying Capacitor [5] as well as H-bridge cascaded [6] inverters, inverters cascaded at either end driving an open-end winding induction motors provide more voltage levels and less output harmonics [7]. Therefore, this topology is gaining popularity in multilevel inverter application and electric driving fields. However, in the case of one single DC power supply operating, zero-sequence circumfluence resulting from zero-sequence voltage generated by inverters cascaded at either end of open-winding induction motors still attracts the interest of many researchers, which mainly focus on dual two-level inverters and dual three-level inverters. To solve this problem, many zero-sequence voltage elimination methods and modulation strategies have been proposed based on dual two-level and dual three-level inverters [8]-[16].

In [17] Srinivasan P et.al proposed an effective method using two isolated DC power supplies to eliminate zero-sequence circumfluence when these two two-level inverters series at either end of the open-end winding induction motor. However, with two extra isolated DC power supplies, the system cost will be excessively high and the implementation of four-quadrant operation is difficult to achieve. Somasekhar V. T. et.al proposed two methods aiming at eliminating zero-sequence voltages. The first one used the unified voltage modulation strategy [18] and the 180° decoupled PWM strategy [19] to adjust the duration of the small vectors so that the mean zero-sequence voltage is zero during each switching cycle. Then the zero-sequence voltage is dynamically eliminated [20]. The other way is the biasing inverter PWM strategy [6] where the mean value of summation of three-phase voltage is zero. Nevertheless, these two methods are without two isolated DC power supplies. However, it is only the average value of the zero-sequence voltage that is eliminated while the instantaneous value is

Manuscript received Apr. 2, 2016; accepted Sep. 7, 2016
Recommended for publication by Associate Editor Lixiang Wei.
†Corresponding Author: 1543152515@qq.com
Tel: +86-15252026403, China University of Mining and Technology
*School of Information and Electrical Engineering, China University of Mining and Technology, China

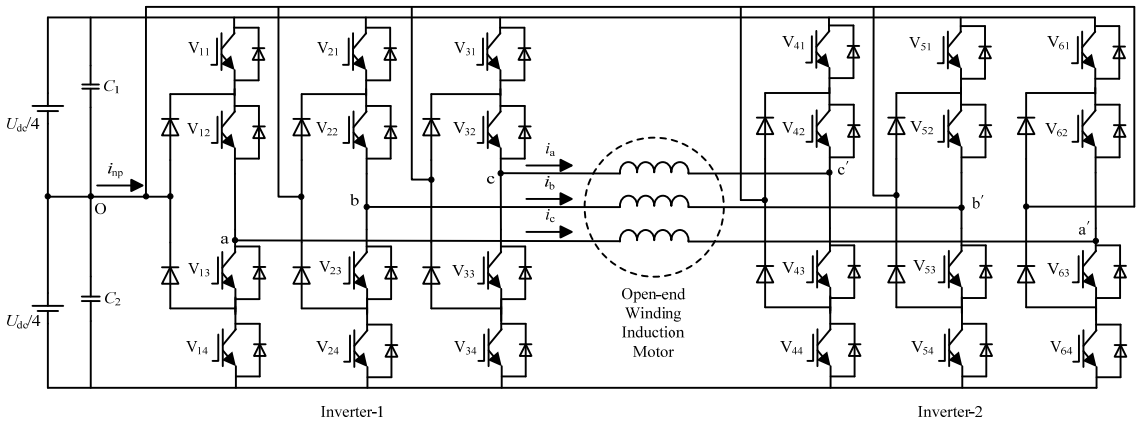

Fig. 1. Topology of dual three-level inverter-fed open-end winding induction-motor with a single DC power supply.

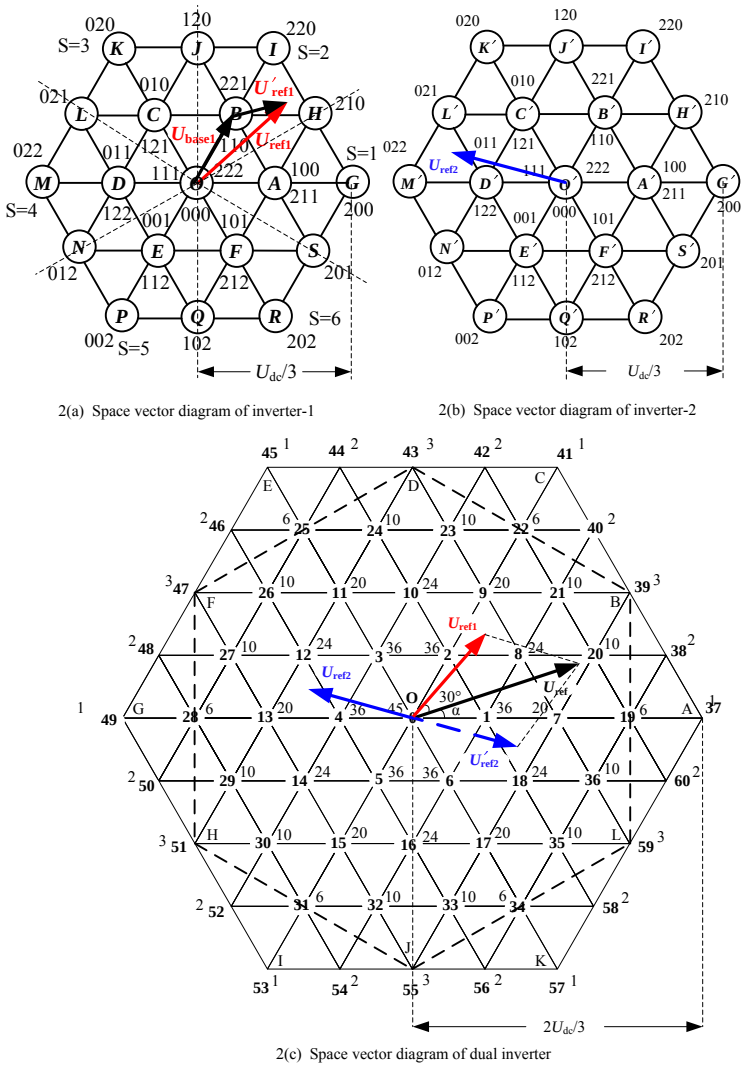

Fig. 2. Principle of space voltage vector 120° decoupling.

still high. The authors of [21] implemented the biasing inverter PWM strategy and the 180° decoupled PWM strategy to eliminate zero-sequence voltage as well as common-mode voltage. However, the instantaneous value is not completely eliminated.

Thus, the unified voltage modulation strategy and the 120° decoupled PWM strategy are applied to resolve the reference voltage vector into two vectors generated by each inverter, with equal size but an angle of 120°, which can completely eliminate instantaneous zero-sequence voltage. The zero-sequence circulating current, which increases the amplitude of the current and brings a lot of damage to the

insulation of the winding, can also be eliminated by the method proposed in this paper. Both simulation and experimental results have verified the correctness and effectiveness of this method.

II. Dual Three-level Inverter Fed Open Winding Induction Motor Drive

The topology of a dual three-level inverter fed open-end winding induction motor drive operated with a single power supply is shown in Fig. 1. It should be noted from this figure that inverter-1 and inverter-2 are in series at either end of the motor. Since both inverters are NPC three-level inverters, each inverter has 27 switching states as shown in Figs. 2(a) and 2(b), respectively. States '0', '1' and '2' in Fig. 2 represent the output voltage level including '$-V_{dc}/4$', '0' and '$V_{dc}/4$', from which 729 switching states are achieved in dual three-level inverters. The corresponding vector diagram is shown in Fig. 2(c) where the uppercase figures are voltage vector number while the superscripts represent the number of redundant switching states. In the meantime, it is also noted that Fig. 2 is same as a vector diagram of a traditional five-level NPC inverter. The only difference is that there are more redundant states in the former case.

Let u_{zs} be the zero-sequence voltage of a dual three-level inverter system and their mathematical relation is [19]:

$$u_{zs} = u_{cm1} - u_{cm2} \tag{1}$$

u_{cm1} and u_{cm2} are the common-mode voltages of inverter-1 and inverter-2 respectively, where $u_{cm1}=(u_{ao}+u_{bo}+u_{co})/3$ and $u_{cm2}=(u_{a'o}+u_{b'o}+u_{c'o})/3$.

When operating in a two isolated DC voltage source mode, even the zero-sequence voltage u_{zs} is excessively large. The DC sources of two inverters are isolated, among which the zero-sequence current is zero due to no circuit. This is a harmless mode and no extra solution is needed for the zero-sequence voltage suppression. However, a closed circuit in the system generates excessive zero-sequence current when operating in a single DC voltage source. Thus, a large circumfluence is formed. As a result, the phase-current harmonics then increase causing insulation damage [17]. In the latter case, the zero-sequence voltage should be suppressed for good operation of the system.

III. The 120° Decoupled PWM Strategy

A. Principles of the 120° Decoupled PWM Strategy

Based on the principles of the decoupled PWM strategy [16], the voltage vector is resolved into two vectors generated by inverter-1 and inverter-2, respectively. As a result, the two inverters are controlled individually. As shown in Fig. 2, the reference voltage vector is $\boldsymbol{U}_{ref}$ ($|\boldsymbol{U}_{ref}|\angle\alpha$) and two equivalent vectors of the same size but with an angle of 60°, $\boldsymbol{U}_{ref1}$($|\boldsymbol{U}_{ref1}|\angle(\alpha+30°)$) and $\boldsymbol{U}'_{ref2}$ ($|\boldsymbol{U}'_{ref2}|\angle(\alpha-30°)$), are achieved using parallelogram law. More specifically, $\boldsymbol{U}_{ref1}$ is generated by inverter-1 while $\boldsymbol{U}'_{ref2}$ is generated by inverter-2. Among these the vector $\boldsymbol{U}_{ref2}$ that is actually needed is in the opposite direction of $\boldsymbol{U}'_{ref2}$ since the directions at either end of the motor are opposite. Thus, $\boldsymbol{U}_{ref1}$ and $\boldsymbol{U}_{ref2}$ actually have a phase difference of 120° and the relations between $\boldsymbol{U}_{ref}$、$\boldsymbol{U}_{ref1}$、$\boldsymbol{U}_{ref2}$ are shown in (2).

It can be noted from the above analysis that the 120° decoupled PWM strategy is an effective way for the independent control of two inverters. Another advantage of such a strategy is that when a fault happens to one of the two inverters, the system can smoothly switch to single inverter supply mode. Thus, the five-level inverter is converted to a three-level inverter. As a result, the induction motor does not have to shut down and stability as well as reliability are increased. It should be noted that the voltage is reduced by $1/\sqrt{3}$ and the system is running under a full load at low speed, when the system operates in a fault-tolerant situation.

$$\begin{aligned} \boldsymbol{U}_{ref} &= \boldsymbol{U}_{ref1} - \boldsymbol{U}_{ref2} \\ |\boldsymbol{U}_{ref1}| &= |\boldsymbol{U}_{ref2}| = \left|\frac{\boldsymbol{U}_{ref}}{\sqrt{3}}\right| \end{aligned} \tag{2}$$

B. Zero-sequence Voltage Elimination

Suppose that the voltage vector $\boldsymbol{U}_{ref}$ is located in the position shown in Fig. 2(c). $\boldsymbol{U}_{ref1}$ and $\boldsymbol{U}_{ref2}$ are achieved by resolving $\boldsymbol{U}_{ref}$ with an angle of 120°, as shown in Figs. 2(a) and 2(b). From the NTV (Nearest Triangle Vector) theory[22], $\boldsymbol{U}_{ref1}$ is composed of three vectors including $B\,H\,I$, while $\boldsymbol{U}_{ref2}$ is composed of $D'\,L'\,M'$. To achieve the operating time of each vector, two equivalent vectors need to be converted to basic vectors and two-level sub-vectors. Then unified voltage modulation is applied to determine the operating vectors and to calculate the operating time of each vector, which is the same as the two-level SVPWM. To simplify this case, take the example of $\boldsymbol{U}_{ref1}$, which is shown in Fig. 2(a).

Let:

$$\boldsymbol{U}_{ref1} = \begin{bmatrix} u_{refa1} & u_{refb1} & u_{refc1} \end{bmatrix} \tag{3}$$

Where u_{refa1}, u_{refb1}, and u_{refc1} are components of $\boldsymbol{U}_{ref1}$ under the abc coordinate system.

The three-level vector diagram can be seen as a combination of six two-level vector diagrams, where the six large sectors are named S, and among each large sector there is a two-level vector diagram. However, the overlapping part of the two-level vector diagram is split evenly into the neighboring parts.

The specific sector judgment rules are shown in Table I.

TABLE I
DISCRIMINATION RULES OF SECTOR

Sector(S)	Criteria
1	$u_{refa1}>0\&u_{refb1}<0\&u_{refc1}<0$
2	$u_{refa1}>0\&u_{refb1}>0\&u_{refc1}<0$
3	$u_{refa1}<0\&u_{refb1}>0\&u_{refc1}<0$
4	$u_{refa1}<0\&u_{refb1}>0\&u_{refc1}>0$
5	$u_{refa1}<0\&u_{refb1}<0\&u_{refc1}>0$
6	$u_{refa1}>0\&u_{refb1}<0\&u_{refc1}>0$

TABLE II
THE THREE-PHASE VAULE OF BASE VECTORS IN DIFFERENT SECTOR

Sector(S)	$\boldsymbol{u}_{basea1}$	$\boldsymbol{u}_{baseb1}$	$\boldsymbol{u}_{basec1}$
1	$U_{dc}/6$	$-U_{dc}/12$	$-U_{dc}/12$
2	$U_{dc}/12$	$U_{dc}/12$	$-U_{dc}/6$
3	$-U_{dc}/12$	$U_{dc}/6$	$-U_{dc}/12$
4	$-U_{dc}/6$	$U_{dc}/12$	$U_{dc}/12$
5	$-U_{dc}/12$	$-U_{dc}/12$	$U_{dc}/6$
6	$U_{dc}/12$	$-U_{dc}/6$	$U_{dc}/12$

A basic vector $\boldsymbol{U}_{base}$ is introduced to map the space vector to the two-level space-vector plane. The new basic vector is the central vector of each sector as shown in Fig. 2(a).

Take $\boldsymbol{U}_{ref1}$ in Fig. 2(a) as an example. Fig. 2(a) shows the position of the equivalent reference voltage vector $\boldsymbol{U}_{ref1}$, where $\boldsymbol{U}_{base1}=\boldsymbol{U}_{110}$ among inverter-1. The adjusted vector $\boldsymbol{U}'_{ref1}$ in the two-level case is:

$$\begin{aligned}&\boldsymbol{U}'_{ref1}=\boldsymbol{U}_{ref1}-\boldsymbol{U}_{base1}\\&\boldsymbol{U}_{base1}=\begin{bmatrix}u_{basea1} & u_{baseb1} & u_{basec1}\end{bmatrix}\end{aligned}\tag{4}$$

Thus:

$$\begin{aligned}&u'_{refa1}=u_{refa1}-u_{basea1}\\&u'_{refb1}=u_{refb1}-u_{baseb1}\\&u'_{refc1}=u_{refc1}-u_{basec1}\\&u'_{refa1}>u'_{refb1}>u'_{refc1}\\&\boldsymbol{U}'_{ref1}=\begin{bmatrix}u'_{refa1} & u'_{refb1} & u'_{refc1}\end{bmatrix}\end{aligned}\tag{5}$$

Similarly, the corrected equivalent voltage vectors under the two-level space-vector plane among the other sectors can be analysed, and the components of central vector of each sector in the abc coordinate system are presented in Table II.

The corrected vectors are two-level vectors. Therefore, the operating time corresponding to the switching states can be calculated by the unified voltage modulation strategy.

Coupled with modified u'_{refa1}, u'_{refb1}, u'_{refc1} and the DC voltage $U_{dc}/2$, the relation between the modulated signal and the output voltage is:

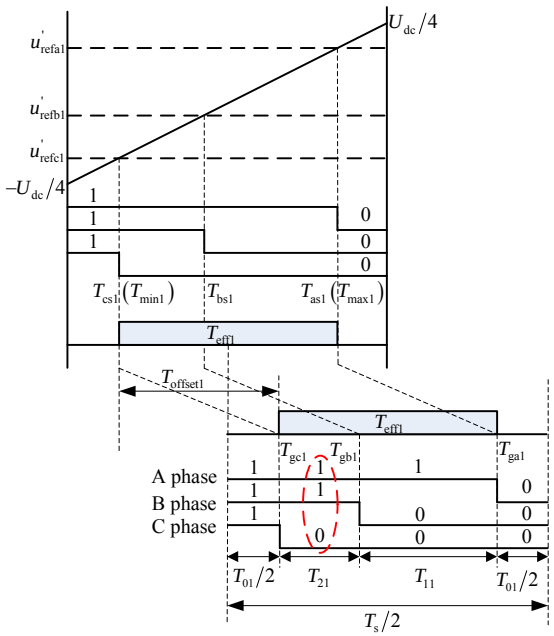

Fig. 3. Functional principle of the unified PWM for $\boldsymbol{U}_{ref1}$.

$$T_{xs1}=\frac{2u'_{refx1}}{U_{dc}}\cdot T_s\tag{6}$$

Where x∈(a, b, c), T_{as1}, T_{bs1} and T_{cs1} are the imaginary switching times for the bridge.

To get the actual switching time of each bridge, define the effective time T_{eff}, which refers to the durations of the different voltage level outputs of the inverter, as is illustrated in Fig. 3.

Let T_{max1} = max(T_{as1}, T_{bs1}, T_{cs1}) and T_{min1} = min(T_{as1}, T_{bs1}, T_{cs1}). T_{eff1} is the effective time of inverter-1. From Fig. 3, it can be achieved that:

$$T_{eff1}=T_{max1}-T_{min1}\tag{7}$$

The actual switching time can be achieved by adding a shifted time $T_{offset1}$ to the imaginary switching time. In the SVPWM effective time T_{eff1} is put at the centre of a half cycle. Thus, the shifted time $T_{offset1}$ is:

$$\begin{aligned}&T_{01}=T_s/2-T_{eff1}\\&T_{offset1}=T_{01}/2-T_{min1}\end{aligned}\tag{8}$$

Therefore, the actual switching times are:

$$T_{gx1}=T_{xs1}+T_{offset1}\tag{9}$$

Where x ∈ (a, b, c), T_{ga1}, T_{gb1} and T_{gc1} are the actual switching instants of the bridge.

Only two switching states (0,1) are achieved through the above strategy. Thus, an inverse-process to map the two-level vectors to three-level vectors is implemented to drive the NPC three-level inverter. That is to say, the real switching

TABLE III
SWITCH STATUS OF THE INNER VECTOR OF DIFFERENT SECTOR

Sector(S)	Switching states of the central vector
1	100
2	110
3	010
4	011
5	001
6	101

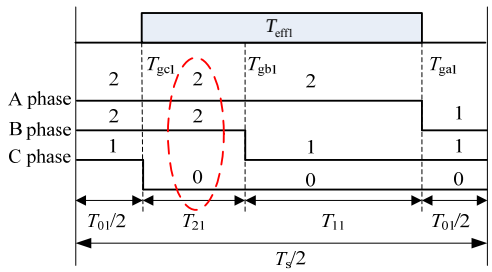

Fig. 4. Instantaneous mapped three-phase reference signals for $\boldsymbol{U}_{\mathbf{ref1}}$, corresponding gating pulses and effective switching time.

states can be obtained by adding a two-level vector to the equivalent central vector of each sector. The switching states of the central vector in each sector are shown in Table III.

Fig. 3 represents the gating pulses of the two level inverter, which is achieved by decomposing the reference vector into the small vector of a two level inverter. Fig. 4 represents the actual states and it can be obtained by the following method. As shown in Fig. (2), it can be find that the reference vector $\boldsymbol{U}_{\mathbf{ref1}}$ is located in sector 2. The central vector in sector 2 is 110. Therefore, the actual switching states of $\boldsymbol{U}_{\mathbf{ref1}}$ are achieved by adding the state 110, to the original two-level states as presented in Fig. 3. For example, the actual state (220) is achieved by adding (110) to (110).

Similarly, $\boldsymbol{U}_{\mathbf{ref2}}$ can be achieved through this method, where the relations between the switching states and the effective time are shown in Fig. 5.

The switching states corresponding to $\boldsymbol{U}_{\mathbf{ref1}}$ are 221-220-210-110, based on the relations between the common-mode voltage and the phase voltage of the inverter. The common-mode voltage of inverter-1 is achieved as (10).

$$\begin{aligned}
u_{\mathrm{cm1}}(221) &= \frac{1}{3}\cdot\left(\frac{U_{\mathrm{dc}}}{2}+\frac{U_{\mathrm{dc}}}{2}+0\right)=\frac{U_{\mathrm{dc}}}{3}\\
u_{\mathrm{cm1}}(220) &= \frac{1}{3}\cdot\left(\frac{U_{\mathrm{dc}}}{2}+\frac{U_{\mathrm{dc}}}{2}-\frac{U_{\mathrm{dc}}}{2}\right)=\frac{U_{\mathrm{dc}}}{6}\\
u_{\mathrm{cm1}}(210) &= \frac{1}{3}\cdot\left(\frac{U_{\mathrm{dc}}}{2}+0-\frac{U_{\mathrm{dc}}}{2}\right)=0\\
u_{\mathrm{cm1}}(110) &= \frac{1}{3}\cdot\left(0+0-\frac{U_{\mathrm{dc}}}{2}\right)=-\frac{U_{\mathrm{dc}}}{6}
\end{aligned} \tag{10}$$

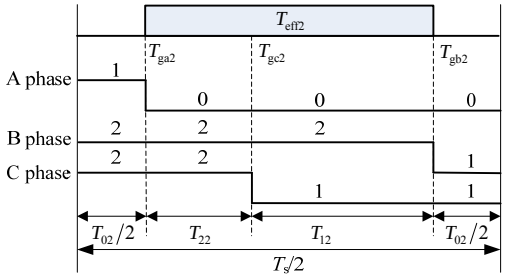

Fig. 5. Instantaneous mapped three-phase reference signals for $\boldsymbol{U}_{\mathbf{ref2}}$, corresponding gating pulses and effective switching time.

The switching states corresponding to $\boldsymbol{U}_{\mathbf{ref2}}$ are 122-022-012-011, which correspond to the common-mode voltage of inverter-2:

$$\begin{aligned}
u_{\mathrm{cm2}}(122) &= \frac{1}{3}\cdot\left(0+\frac{U_{\mathrm{dc}}}{2}+\frac{U_{\mathrm{dc}}}{2}\right)=\frac{U_{\mathrm{dc}}}{3}\\
u_{\mathrm{cm2}}(022) &= \frac{1}{3}\cdot\left(-\frac{U_{\mathrm{dc}}}{2}+\frac{U_{\mathrm{dc}}}{2}+\frac{U_{\mathrm{dc}}}{2}\right)=\frac{U_{\mathrm{dc}}}{6}\\
u_{\mathrm{cm2}}(012) &= \frac{1}{3}\cdot\left(-\frac{U_{\mathrm{dc}}}{2}+0+\frac{U_{\mathrm{dc}}}{2}\right)=0\\
u_{\mathrm{cm2}}(011) &= \frac{1}{3}\cdot\left(-\frac{U_{\mathrm{dc}}}{2}+0+0\right)=-\frac{U_{\mathrm{dc}}}{6}
\end{aligned} \tag{11}$$

Based on the mathematical relationship between $\boldsymbol{U}_{\mathbf{ref1}}$ and $\boldsymbol{U}_{\mathbf{ref2}}$, shown in Figs. 2(a) and 2(b), it is known that:

$$\begin{aligned}
T_{01} &= T_{02}\\
T_{11} &= T_{12}\\
T_{21} &= T_{22}
\end{aligned} \tag{12}$$

In the meantime, the operating vectors are achieved through (1) and the zero-sequence voltage among the 4 operating durations, $T_{01}/2(T_{02}/2)$、T_{21} (T_{22})、T_{11} (T_{12})、$T_{01}/2$ $(T_{02}/2)$, which are presented in (13).

$$\begin{aligned}
u_{\mathrm{zs}}\left(\frac{T_{01}}{2}\right) &= \frac{u_{\mathrm{cm1}}-u_{\mathrm{cm2}}}{3}\\
&= \frac{U_{\mathrm{dc}}/3-U_{\mathrm{dc}}/3}{3}=0\\
u_{\mathrm{zs}}(T_{21}) &= \frac{u_{\mathrm{cm1}}-u_{\mathrm{cm2}}}{3}\\
&= \frac{U_{\mathrm{dc}}/6-U_{\mathrm{dc}}/6}{3}=0\\
u_{\mathrm{zs}}(T_{11}) &= \frac{u_{\mathrm{cm1}}-u_{\mathrm{cm2}}}{3}\\
&= \frac{0-0}{3}=0\\
u_{\mathrm{zs}}\left(\frac{T_{01}}{2}\right) &= \frac{u_{\mathrm{cm1}}-u_{\mathrm{cm2}}}{3}\\
&= \frac{-U_{\mathrm{dc}}/6-(-U_{\mathrm{dc}}/6)}{3}=0
\end{aligned} \tag{13}$$

From the above discussion, the zero-sequence voltage of an open-end winding induction motor during each duration of a

half cycle is zero. Additionally, due to the symmetry of seven-segment modulation, it can be concluded that during one cycle the instantaneous value of the zero-sequence voltage is zero. Similarly, when the reference voltage $\boldsymbol{U}_{\mathbf{ref}}$ arrives at other positions, as shown in Fig. 2(c), the instantaneous value of the zero-sequence voltage during each operating period among each cycle is zero.

It can be concluded that with the implementation of the 120° decoupled PWM strategy, the instantaneous value of the zero-sequence voltage in an open-end winding induction motor can be completely eliminated. Compared with the 180° decoupled PWM strategy proposed in [20], the method presented in this paper is essentially different since it is the instantaneous value that is eliminated while [20] aimed at eliminating the mean value. Thus, when operating in the single DC source mode, the harmonics content is not affected and good performance of the system is achieved by the strategy proposed in this paper.

C. Modulation Range Analysis

Strategies implemented to eliminate zero-sequence voltage will have certain effects on the linear modulation range.

Let |OA|=2U_{dc}/3, as shown in Fig. 2(c), then |OG|=|O′ G′ |=U_{dc}/3, which is shown in Fig. 2(a) and Fig. 2(b). The modulation range of the system without the 120° decoupled PWM strategy corresponds to the regular hexagon *ACEGIK*, among which the maximum amplitude of the phase voltage generated by the dual three-level inverters is $U_{dc}/\sqrt{3}$.

When the 120° decoupled PWM strategy is applied to the system, each basic vector of the vector diagrams of the dual three-level inverter is composed of two three-level vectors, with a maximum amplitude of |OG|=U_{dc}/3, with an angle of 120°. Thus, the maximum amplitude of the basic vector is |OB|=$U_{dc}/\sqrt{3}$. As can be seen from Fig. 2(c), the modulation area is reduced to an inscribed regular hexagon *BDFHJL*, among which the maximum amplitude of the modulated phase-voltage is U_{dc}/2. As a result, the linear modulation range of the system implementing zero-voltage elimination is reduced by:

$$\frac{U_{dc}/\sqrt{3}-U_{dc}/2}{U_{dc}/\sqrt{3}}\times 100\% = 13.4\% \tag{14}$$

As shown in (15), the DC voltage then needs to be increased to obtain the same maximum output phase-voltage amplitude as the traditional five-level NPC inverter.

$$\frac{2U_{dc}/\sqrt{3}-U_{dc}}{U_{dc}}\times 100\% = 15.5\% \tag{15}$$

Originally the DC bus voltage of dual three-level inverters is only half that of a five-level NPC inverter. Thus, even the same maximum output phase-voltage as a five-level inverter is achieved, and the dual three-level inverters' DC voltage is only 57.75% of that for a five-level NPC inverter.

TABLE IV
SIMULATION PARAMETERS SETTING FOR OPEN-END WINDING INDUCTION-MOTOR

Parameters	Value
Rated power of motor	5.5 kW
Rated voltage of motor	380 V
Rated current of motor	12.1 A
Rated frequency of motor	50 Hz
Rated speed of motor	1460 rpm
Stator resistance of motor	1.844Ω
Stator inductance of motor	11.31 mH
Rotor resistance of motor	1.826 Ω
Rotor inductance of motor	11.31 mH
Mutual inductance between stator and rotor	104.83 mH
Moment of Inertia	0.021 kg.m^2
Number of pole-pairs	2

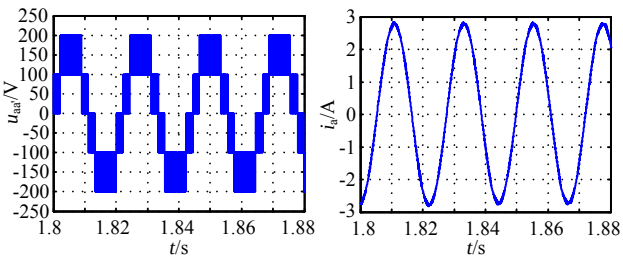

Fig. 6. Simulation result of motor phase current and phase voltage for modulation indices of m_a = 0.9.

IV. SIMULATION AND EXPERIMENT RESEARCH

A. Simulation Research

A simulation model in MATLAB/Simulink is established to verify the effectiveness of the proposed zero-sequence elimination method. The induction motor is controlled by the V/F, and the DC voltage of the inverter is set to 200V while the carrier frequency is 5kHz. Table IV presents the specific parameters of the simulation.

Define the modulation ratio as m_a=2U_{ref}/U_{dc}. When m_a is 0.9, the phase current i_a and voltage u_{aa} waveforms, supplied by a single DC source, are shown in Fig. 6. When m_a is 0.4 and the system is operating under a single DC source, the phase current i_a and voltage $u_{aa'}$ waveforms are shown in Fig. 7.

To further demonstrate the effectiveness of the 120° PWM strategy, simulation results of the zero-sequence voltage are shown when operating on a single DC source, with m_a values of 0.9 and 0.4 respectively, the waveforms of which are shown in Fig. 8. Then let the dual three-level inverters operate on high and low modulation depths and implement

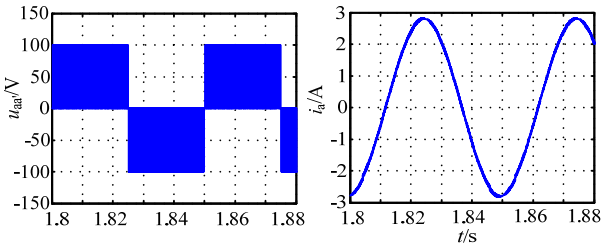

Fig. 7. Simulation result of motor phase current and phase voltage for modulation indices of $m_a = 0.4$.

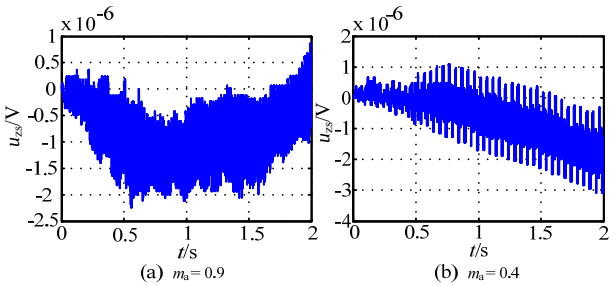

Fig. 8. Simulation result of zero-sequence voltage in dual three-level inverter-fed open-end winding motor for modulation indices of $m_a = 0.9$ and $m_a = 0.4$ with a single DC power supply.

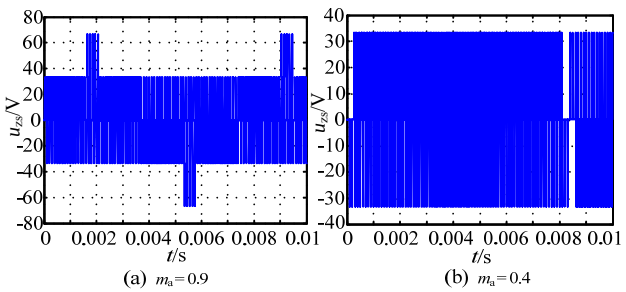

Fig. 9. Simulation result of zero-sequence voltage in dual three-level inverter-fed open-end winding motor for modulation indices of $m_a = 0.9$ and $m_a = 0.4$ by using space voltage vector 180° decoupling.

the 180° decoupled space vector PWM strategy presented in [20]. Thus, the simulation waveforms of the zero-sequence voltage are finally achieved in Fig. 9.

From Figs. 6, 7 and 8, it can be seen that with the implementation of the 120° decoupled PWM strategy, operating on different modulation ratios, the output phase-voltage is five-level during the high modulation range, and it turns into three-level during the low modulation range. The good thing is that in both cases the output current waveforms are quite favorable and the instantaneous value of the zero-sequence is zero. However, the results from Fig. 9 show that the strategy in [20] mainly eliminates the mean value while the high-frequency zero-sequence voltage still exists, with a large amplitude. Therefore, it can concluded that there is an essential difference between the strategies proposed in this paper and in [20].

B. Experiment Research

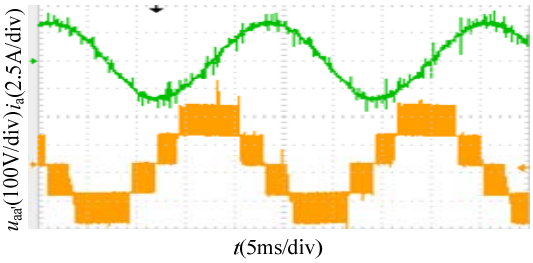

Fig. 10. Experimental result of motor phase current and phase voltage for modulation indices of $m_a = 0.9$. Upper trace: motor phase current i_a, Lower trace: motor phase voltage $u_{aa'}$.

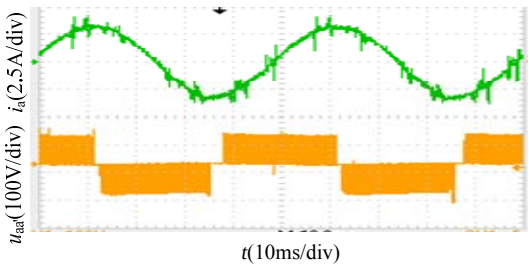

Fig. 11. Experimental result of motor phase current and phase voltage for modulation indices of $m_a = 0.4$. Upper trace: motor phase current i_a, Lower trace: motor phase voltage $u_{aa'}$.

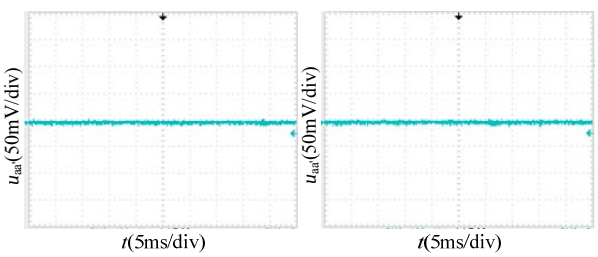

Fig. 12. Experimental result of zero-sequence voltage in dual three-level inverter-fed open-end winding motor for modulation indices of $m_a = 0.9$ and $m_a = 0.4$ with a single DC power supply.

A 5.5kW dual three-level inverter fed open-end winding induction motor experiment is implemented to verify the effectiveness of the proposing strategy. Two NPC three-level inverters are series connected at either end of the induction motor and an open-looped V/F is applied to the control motor. The controller utilizes a TMS320F28335 to produce 12 PWM pulses. Then a XC3S400 FPGA is used for the inversion of the generated pulses. In total, 24 PWM pulses are generated to drive the dual three-level inverters. The experiment parameters are identical to those of the simulation.

Fig. 10 presents the experimental phase-current i_a and phase-voltage $u_{aa'}$ waveforms under a single DC source when m_a is 0.9. Similarly, when m_a is 0.4 the output phase-current and phase-voltage waveforms are shown in Fig. 11. To observe the zero-sequence voltage waveforms, experiments in the single DC source mode are conducted with two different m_a values of 0.9 and 0.4, the waveforms of which are shown in Fig. 12.

The results from the experiments verify that, under either mode, when operating in the high modulation area the output phase-voltage is five level, otherwise a three-level phase-voltage is achieved. This is similar to the results of the simulation, which show that the instantaneous value of the zero-sequence voltage is zero in either the high or low modulation area. Therefore, the strategy proposed in this paper is effective for completely eliminating zero-sequence voltage.

V. CONCLUSIONS

A new and effective strategy was proposed for the zero-sequence elimination of dual three-level inverter fed open-end winding induction motors, which is achieved by suppressing the instantaneous value. Simulation and experimental results confirm that:

(1) The 120° decoupled PWM strategy can achieve independent control of two inverters and eliminate the instantaneous value of the zero-sequence voltage, which ensure the good performance of systems operating in the single DC source mode.

(2) Compared with the traditional modulation strategy, the linear modulation range of a system implementing zero-voltage elimination is obviously reduced by 13.4%. However, the DC bus voltage of dual three-level inverters is only half that of a five-level NPC inverter. Thus, even if the same maximum output phase-voltage as a five-level inverter is achieved, the dual three-level inverters' DC voltage is only 57.75% of that of a five-level NPC inverter.

(3) To suppress the mean value of zero-sequence voltage, the 180° decoupled space vector PWM strategy needs to calculate and analyze the shifted time, which is more complex than the strategy proposed in this paper.

REFERENCES

[1] A. Nabae, I. Takahash, and H. Akagi, "A new neutral point clamped PWM inverter," *IEEE Trans. Ind. Appl.*, Vol. IA-17, No. 5, pp. 518-523, Sep. 1981.

[2] M. M. Renge and H. M. Suryawanshi, "Multilevel inverter to reduce common mode voltage in AC motor drives using SPWM technique," *Journal of Power Electronics*, Vol. 11, No. 1, pp. 21-27, Jan. 2011.

[3] J. Liu, X. G. Yi, and Z. Zhang, "Key technologies of main circuit topology improvement and PWM security and stability of high-voltage," *Transactions of China Electrotechnical Society*, Vol. 27, No. 8, pp. 28-34, Aug. 2012.

[4] H. B. Hu, W. X. Yao, and Z. Y. Lu, "Realization of three-level SVPWM using FPGA," *Transactions of China Electrotechnical Society*,Vol. 25, No. 5, pp. 116-122, May 2010.

[5] T. A. Maynard and H. Foch, "Multi-level conversion: high voltage choppers and voltage source inverters," in *23rd Annual IEEE Power Electronics Specialists Conference (PESC)*, pp. 397-403, Jun./Jul. 1992.

[6] L. M. Tolbert, F. Z. Peng, and T. G. Habetler, "Multilevel converters for large electric drives," *IEEE Trans. Ind. Appl.*, Vol. 35, No. 1, pp. 36-44, Jan./Feb. 1999.

[7] P. Srinivasan, "A new SVPWM for dual-inverter fed three-level induction motor drive," in *Proceedings of International Conference on Green Computing, Communication and Conservation of Energy (ICGCE)*, pp. 514-518, 2013.

[8] V. T. Somasekhar, K. Gopakumar, A. Pittet, and V. T. Ranganathan, "PWM inverter switching strategy for a dual two-level inverter fed open-end winding induction motor drive with a switched neutral," in *IEE Proceedings - Electric Power Applications*, Vol. 149, No. 2, pp. 152-160, Mar. 2002.

[9] V. T. Somasekhar, M. R. Baiju, and K. Gopakumar, "Dual two level inverter scheme for an open-end winding induction motor drive with a single DC power supply and improved DC bus utilization," *IEE Proceedings – Electric Power Applications*, Vol. 151, No. 2, pp. 230-238, Mar. 2004.

[10] V. T. Somasekhar, K. Gopakumar, and E. G. Shivakumar, "A space vector modulation scheme for a dual two level inverter fed an open-end winding induction motor drive for the elimination of zero sequence currents," *European Power Electronics and Drives*, Vol. 12, No. 2, pp. 26-36, Dec. 2002.

[11] M. R. Baiju, K. K. Mohapatra, R. S. Kanchan, and K. Gopakumar. "A dual two-level inverter scheme with common mode voltage elimination for an induction motor drive," *IEEE Trans. Power Electron.*, Vol. 19, No. 3, pp. 794-805, May 2004.

[12] V. Oleschuk, A. Sizov, B. K. Bose, and A. M. Stankovic, "Phase shift based synchronous modulation of dual-inverters for an open-end winding induction motor drive with elimination of zero sequence currents," in *International Conference on Power Electronics and Drive Systems (PEDS)*, Nov./Dec. 2005.

[13] V. T. Somasekhar and S. Srinivas. "Switching algorithms for a dual inverter fed open-end winding induction motor drive," in *Proceedings of IEEE India International Conference on Power Electronics*, 2004.

[14] V. T. Somasekhar, S. Srinivas, and K. Gopakumar. "A space vector based PWM switching scheme for the reduction of common-mode voltages for a dual inverter fed open-end winding induction motor drive," in *IEEE 36th Power Electronics Specialists Conference (PESC)*, Jun. 2005.

[15] S. Srinivas and V. T. Somasekhar. "A new alternate-inverter PWM switching strategy for reducing the common-mode voltages for a dual-inverter fed open-end winding induction motor drive," in *Proceedings of Power Electronics Specialists Conference*, pp. 1460-1465, 2005.

[16] V. T. Somasekhar, S. Srinivas, and B. P. Reddy, "PWM switching strategy for the dynamic balancing of zero-sequence current for a dual-inverter fed open-end winding induction motor drive," *IEEE Electric on Power Applications*, Vol. 1, No. 4, pp. 591-600, Jul. 2007.

[17] S. Pradabane, B. L. Narasimharaju, and N. V. Srikanth, "Two-quadrant clamping inverter scheme for three-level open-end winding induction motor drive," in *IEEE International Conference on Power Electronics, Drives and Energy Systems (PEDES)*, Dec. 2014.

[18] D. W. Chung, J. S. Kim, and S. K. Sul, "Unified voltage

modulation technique for real-time three-phase power conversion," *IEEE Trans. Ind. Appl.*, Vol. 34, No. 2, pp. 374-380, Mar./Apr. 1998.

[19] S. Srinivas and V. T. Somasekhar, "Switching algorithms for the dual inverter fed open-end winding induction motor drive for 3-level voltage space phasor generation," *Asian Power Electronics Journal*, Vol. 1, No. 1, pp. 96-110, Aug. 2007.

[20] V. T. Somasekhar, S. Srinivas, and K. K. Kumar, "Effect of zero-vector placement in a dual-inverter fed open-end winding induction-motor drive with a decoupled space-vector PWM strategy," *IEEE Trans. Ind. Electron*., Vol. 55, No. 6, pp. 2497-2505, Jun. 2008.

[21] D. Wu, L. C. Su, X. J. Wu, and G. D. Zhao, "An optimized control method based on dual three-level inverters for open-end winding induction motor drives," *Journal of Power Electronics*, Vol. 14, No. 2, pp. 315-323, Mar. 2014.

Yi-Wen Geng was born in Jiangsu Province, China, in 1977. He received his B.S. and M.S. degrees in Electrical Engineering from the China University of Mining and Technology, Xuzhou, China, in 2000 and 2004, respectively. He has been with the Department of Information and Electrical Engineering, China University of Mining and Technology, where he is presently working as an Associate Professor. His current research interests include PV inverters, harmonic control and power electronics.

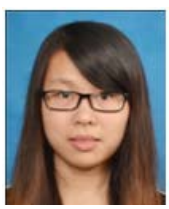

Chen-Xi Wei was born in Shandong Province, China, in 1993. She received her B.S. degree in Electrical Engineering from the China University of Mining and Technology, Xuzhou, China, in 2015. She is presently working towards her M.S. degree in Electrical Engineering in School of Information and Electrical Engineering, China University of Mining and Technology. Her current research interests include the advanced control of ac machines, the modulation of multi-level inverters, and power electronics.

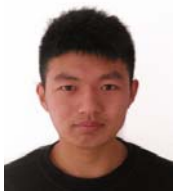

Rui-Cheng Chen was born in Jiangsu Province, China, in 1992. He received his B.S. degree in Electrical Engineering from the China University of Mining and Technology, Xuzhou, China, in 2015. He is presently working towards his M.S. degree in Electrical Engineering in School of Information and Electrical Engineering, China University of Mining and Technology. His current research interests include the control of double three-phase permanent magnet synchronous motors, the modulation of multi-level inverters, and power electronics.

Liang Wang was born in Jiangsu Province, China, in 1992. He received his B.S. degree in Electrical Engineering from the China University of Mining and Technology, Xuzhou, China, in 2014. He is presently working towards his M.S. degree in Electrical Engineering in School of Information and Electrical Engineering, China University of Mining and Technology. His current research interests include power electronics and electrical drives.

Jia-Bin Xu was born in Jiangsu Province, China, in 1991. He received his B.S. degree in Electrical Engineering from the China University of Mining and Technology, Xuzhou, China, in 2014. He is presently working towards his M.S. degree in Electrical Engineering in the Department of Information and Electrical Engineering, China University of Mining and Technology. His current research interests include the advanced control of ac machines, the modulation of multi-level inverters, and power electronics.

Shuang-Cheng Hao was born in Jiangsu Province, China, in 1991. He received his B.S. degree in Electrical Engineering from the China University of Mining and Technology, Xuzhou, China, in 2014. He is presently working toward his M.S. degree in Electrical Engineering in the Department of Information and Electrical Engineering, China University of Mining and Technology. His current research interests include power electronics and electrical drives.